To appear in *Advanced Robotics*
Vol. 00, No. 00, Nov 2016, 1–25

FULL PAPER

Decoupling and Tracking Control for Elastic Joint Robots with Coupled Joint Structure

Luc Le-Tien [a*] and Alin Albu-Schäffer[b]

[a] *Robotics and Mechatronics Center, German Aerospace Center (DLR), D-82234 Wessling, Germany*;
[b] *Robotics and Mechatronics Center, German Aerospace Center (DLR) and Department of Informatics, Technical University of Munich, Germany*

(*v2.0 released Nov 2016*)

The paper deals with the modeling, identification and control of a flexible joint robot developed for medical applications at the German Aerospace Center (DLR). In order to design anthropomorphic kinematics, the robot uses a coupled joint structure realized by a differential gear-box, which however leads to strong mechanical couplings inside the coupled joints and must be taken into account. Therefore, a regulation MIMO state feedback controller based on modal analysis is developed for each coupled joint pair, which consists of full state feedback (motor position, link side torque, as well as their derivatives). Furthermore, in order to improve position accuracy and simultaneously keep good dynamic behavior of the MIMO state feedback controller, a cascaded tracking control scheme is proposed, based on the MIMO state feedback controller with additional feedforward terms (desired motor velocity, desired motor acceleration, derivative of the desired torque), which are computed in a computed torque controller and take the whole rigid body dynamics into account. Stability analysis is shown for the complete controlled robot. Finally, experimental results with the DLR medical robot are presented to validate the practical efficiency of the approaches.

Keywords: Flexible joint robots, MIMO state feedback control, decoupling based control, modal control, tracking control.

1. Introduction

The DLR medical robot is developed for medical robotics applications, such as minimally invasive surgery [1], orthopedy [2], or osteotomy. It is a redundant robot with seven degrees of freedom, whose joints are endowed, in addition to the motor position sensors, with torque sensors and link side position sensors which are mounted after the gear box. In order to obtain an anthropomorphic robot design, wrist, elbow and shoulder are realized as coupled joint pairs using a differential gear after a harmonic drive gear unit with high gear ratio for each motor. In this way, the torque of both motors can be used in the principal directions of motion (e.g. the vertical plane), permitting an increase of available torque for a given motor size and thus the reduction of the total weight. Hence, the accelerated masses are relatively low, which permits a safe robot interaction with the human and the environment. Simultaneously, this causes high friction, high joint elasticity and additionally a strong coupling inside the coupled joint pair. As a consequence this leads to strong vibrations and tracking problems of the robot which has to be taken into account in the modeling and the control design.

Many control methods have been proposed for control problems of flexible joint robots. As a simple set point control scheme, a PD controller was introduced in [3] (or with on-line gravity

*Corresponding author. Email: Luc.Le-Tien@dlr.de

compensation in [4]) which uses merely motor position and motor velocity and can be easily implemented. By using a disturbance observer for friction compensation, a PD controller based on nominal states (estimated motor position and motor velocity) was proposed in [5] to achieve global asymptotic stability. Furthermore, in order to effectively damp oscillations of the link side, a SISO state feedback controller was introduced in [6] with full state feedback and friction compensation based on a static friction model. This controller is very robust and successfully applied to the DLR lightweight robots [7]. However, in case of the DLR medical robot with the strong joint coupling within the coupled joint pair (considered by symmetric positive definite joint stiffness, joint damping, and mass matrix) and the high joint elasticity, these set point controllers can not achieve a good dynamic behavior.

For tracking control some advanced controllers were proposed, such as singular perturbation approaches in [8, 9], backstepping approaches in [10, 11], state feedback linearization approaches in [12], cascaded approach using the joint torque feedback in [13], and passivity-based approaches in [14, 15], using either full or partial state feedback. A combination between a partial state feedback linearization technique and a backstepping design method was introduced in [16] to reach a global output tracking control. Furthermore, an alternative control method based on disturbance observer [17–19] was developed for robotic systems. In [20, 21] nonlinear observer based controllers were proposed for flexible joint robots. In order to deal with uncertainties on the robot parameters, adaptive control schemes were introduced in [10, 13, 22]. Based on cascaded analysis, in [23] a robust adaptive control scheme was introduced by using the sliding mode technique. In consideration of the friction effects, in [25] an adaptive control scheme was developed using a static friction model.

Although these advanced control schemes provide high position accuracy, due to the requirement of high derivatives of the link side position they can hardly achieve a good dynamic behavior and are not robust enough for robots with high DOF.

In consideration of the joint elasticity and the joint coupling of the DLR medical robot, this paper firstly extends the method from [6] by using modal analysis to decouple the dynamics of the coupled joints. In this way a simple MIMO state feedback controller is built with full state feedback (motor position, joint torque and their derivatives). In order to avoid chattering effects due to Coulomb friction at zero velocity, a LuGre friction model [24] is used for model-based friction compensation. Furthermore, based on these control parameters, we propose a cascaded tracking control scheme with two control loops[1]. The inner control loop is a MIMO state feedback controller with additional feedforward terms and the outer control loop is a computed torque controller. Thus high position accuracy and good dynamic behavior can be simultaneously achieved. The system stability is derived using Lyapunov approaches and the Krasovskii-LaSalle principle in case of the regulation scheme or Barbalat's lemma in case of the tracking scheme.

[1]Preliminary results were presented in our previous work [26] and [27]. However, this paper presents more explicit and extensive results. Furthermore, the identification of the coupled joint is added.

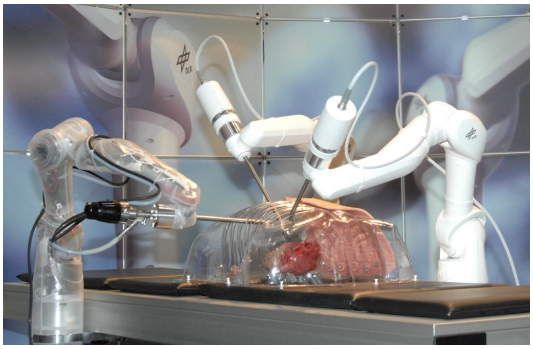

Figure 1. DLR medical robots.

The content of this paper is structured as follows: In Sec. 2, the model of the DLR medical robot with the coupled joints is described. For the set point control, the design of a MIMO state feedback controller based on modal decomposition is introduced in Sec. 3. For the tracking control, a cascaded control scheme based on the MIMO state feedback controller with additional feedforward terms is presented in Sec. 4. Finally, in Sec. 5, identification and experimental results are presented and discussed.

2. Modeling of the DLR medical robot

The first joint of the DLR medical robot is very similar to a joint of the DLR lightweight robot, while a coupled design was chosen for the joint pairs 2-3, 4-5, 6-7 by using differential gear-box (Fig. 2). Therefore, a movement of one coupled joint has to be realized by the coordinated movement of two actuators.

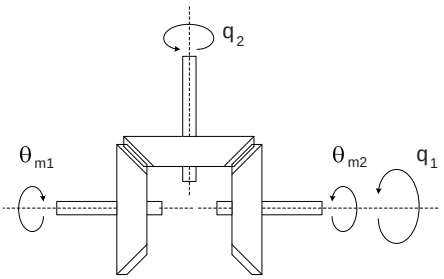

Figure 2. Structure of the differential gear-box.

2.1 *Modeling of the Differential Gear-Box*

Ignoring the elasticity, the effect of the gear-box can be described by the following transformations of the positions and the concerning torques

$$\theta_i = T_i \theta_{m_i} \tag{1}$$

$$\tau_{m_i} = T_i^T \tau_i \tag{2}$$

with transformation matrix

$$T_i = \begin{bmatrix} 0.5 & 0.5 \\ -0.5 & 0.5 \end{bmatrix}, \quad \forall\ i = \{2\_3, 4\_5, 6\_7\}^1. \tag{3}$$

Thereby, the motor position in *motor coordinates* is denoted by θ_{m_i}, while θ_i is the same position expressed in *link coordinates*. It is important to note the difference between the motor position expressed in link coordinates θ_i and the link position, which will be denoted by q_i. While θ_i represents the same system state as θ_{m_i} only written in another coordinate system, the second value q_i is a different state variable, representing the position of the link after the joint elasticity and can also be expressed in motor or link coordinates. Accordingly, τ_i and τ_{m_i} are the joint torques expressed in link and motor coordinates respectively.

[1] $i = \{2\_3, 4\_5, 6\_7\}$ for coupled joint 2-3, 4-5, 6-7.

Furthermore, the transformation matrix for the entire robot is expressed as

$$T = \begin{bmatrix} 1 \ldots & & 0 \\ & T_i & \\ \vdots & & \vdots \\ & T_i & \\ 0 \ldots & & T_i \end{bmatrix} \quad \in \mathbb{R}^{7\text{x}7},\ \forall\ T_i \in \mathbb{R}^{2\text{x}2}. \tag{4}$$

2.2 *Modeling of the Robot Dynamics*

For modeling the entire DLR medical robot based on the flexible joint model, the following dynamic model is used

$$I_m = K_{T2I} u_m \tag{5}$$

$$u_m = J_m \ddot{\theta}_m + T^T(\tau + DK^{-1}\dot{\tau}) + \tau_{fm} \tag{6}$$

$$\tau + DK^{-1}\dot{\tau} = M(q)\ddot{q} + C(q,\dot{q})\dot{q} + g(q) \tag{7}$$

$$\tau = K(T\theta_m - q). \tag{8}$$

Thereby, $I_m \in \mathbb{R}^n$ and $K_{T2I} \in \mathbb{R}^{n\text{x}n}$ are the motor current and the motor constant transforming moment to current respectively. The motor torque $u_m \in \mathbb{R}^n$ is the input quantity for the controller. $J_m \in \mathbb{R}^{n\text{x}n}$ is a diagonal matrix containing the motor inertias. $\tau_{fm} \in \mathbb{R}^n$ is the motor friction torque. The joint torque vector $\tau \in \mathbb{R}^n$ is defined by the linear relation $\tau = K(T\theta_m - q)$, where the joint stiffness matrix $K \in \mathbb{R}^{n\text{x}n}$ (as well as the joint damping matrix $D \in \mathbb{R}^{n\text{x}n}$) is positive definite and symmetric and $K = diag(K_1, K_{2\_3}, K_{4\_5}, K_{6\_7})$ with $\{K_1 \in \mathbb{R},\ K_i \in \mathbb{R}^{2\text{x}2} |\ i \in \{2\_3, 4\_5, 6\_7\}\}$.

Furthermore, $M(q) \in \mathbb{R}^{n\text{x}n}$, $C(q,\dot{q}) \in \mathbb{R}^{n\text{x}n}$ and $g(q) \in \mathbb{R}^n$ are the mass matrix, the vector of Coriolis and centrifugal terms and the gravity term of the rigid robot dynamics.

The following properties of the robot model will be used in this paper

P.1 *The mass matrix is symmetric and positive definite*

$$M(q) = M(q)^T > 0 \quad \forall\ q \in \mathbb{R}^n. \tag{9}$$

P.2 *The matrix $\dot{M}(q) - 2C(q,\dot{q})$ is skew symmetric and satisfies:*

$$x^T(\dot{M}(q) - 2C(q,\dot{q}))x = 0 \quad \forall\ x, q, \dot{q} \in \mathbb{R}^n. \tag{10}$$

P.3 *The gravity torque $g(q)$ is given as the gradient of a potential function $U_g(q)$ so that $g(q) = \partial U_g(q)/\partial q$ and there exists a real number $\alpha > 0$ (see Appendix), such that*

$$\|g(q_1) - g(q_2)\| \leq \alpha \|q_2 - q_1\| \quad ,\ \forall\ q_1, q_2 \in \mathbb{R}^n \tag{11}$$

holds, implying

$$\|U_g(q_d) - U_g(q) + (q - q_d)^T g(q_d)\| \leq \frac{1}{2}\alpha \|q - q_d\|^2. \tag{12}$$

P.4 *Based on the LuGre friction model in [24] and in consideration of the load effect on the joint elasticity, the following friction model is used*

$$\tau_{fm} = \sigma_0 z + \sigma_1 \dot{z} + f_v \dot{\theta}_m \tag{13}$$

with the inner dynamics

$$\begin{cases} \dot{z} = \dot{\theta}_m - \frac{|\dot{\theta}_m|}{h_z}\sigma_0 z \\ h_z = f_c + f_l \mid \tau_m \mid . \end{cases} \tag{14}$$

Thereby, z is the inner state of the LuGre friction model. σ_0, σ_1, f_c, f_v and f_l represent the stiffness, damping, Coulomb, viscous and load dependent coefficients, respectively.

3. MIMO state feedback controller without feedforward terms

3.1 *Modal Analysis for Control Design*

In this section, the following lemma [30] is used to diagonalize two matrices.

Lemma 1 *(Decomposition of symmetric matrices): Given a symmetric matrix K, and a symmetric, positive definite matrix M, there exists an invertible matrix Q, such that $K = QQ^T$ and $M = QM_QQ^T$ holds, with the matrix M_Q being diagonal.*

As known from modal analysis, a mechanical system of the form

$$f = M\ddot{x} + Kx \tag{15}$$

with f and x being a generalized force and the state vector. Using the previous lemma, (15) can be transformed into the so called modal coordinates in which the system is decoupled. So one obtains the decoupled equation

$$f_Q = M_Q\ddot{x}_Q + x_Q. \tag{16}$$

with $x_Q = Q^Tx$ and $f_Q = Q^{-1}f$.

In order to apply the idea to the flexible joint robot, let us rewrite (6) in link coordinates

$$u = J\ddot{\theta} + \tau + DK^{-1}\dot{\tau} \tag{17}$$

with

$$\theta = T\theta_m \tag{18}$$

$$u = T^{-T}(u_m - \tau_{fm}) \tag{19}$$

$$J = T^{-T}J_mT^{-1}. \tag{20}$$

Notice that (20) is a congruence transformation, preserving symmetry and positive definiteness of the matrix.

For the linear control design let us now consider the linearized model of a coupled joint pair i around a worst case position (e.g. maximum inertia)[1]

$$\overline{u}_i = J_i\ddot{\overline{\theta}}_i + \overline{\tau}_i + D_iK_i^{-1}\dot{\overline{\tau}}_i \tag{21}$$

$$\overline{\tau}_i + D_iK_i^{-1}\dot{\overline{\tau}}_i = M_{d_i}\ddot{\overline{q}}_i \tag{22}$$

[1]In the considered equilibrium the linearization of the rigid-body dynamics is given by

$$K(\overline{\theta} - \overline{q}) + D(\dot{\overline{\theta}} - \dot{\overline{q}}) = M(q_d)\ddot{\overline{q}} + K_g\overline{q} \quad \text{or} \quad K(\overline{\theta} - K^{-1}(K + K_g)\overline{q}) + D(\dot{\overline{\theta}} - \dot{\overline{q}}) = M_d\ddot{\overline{q}}$$

with $M_d \equiv M(q_d)$ and $K_g = \frac{\partial g(q)}{\partial q}\Big|_{q=q_d}$. Because DLR medical robot's ratio $K_{jj}/|K_{g_{jj}}| > 50$, follows $K^{-1}(K + K_g) \approx I$.

with $\{\overline{\theta}, \dot{\overline{\theta}}, \ddot{\overline{\theta}}, \overline{q}, \dot{\overline{q}}, \ddot{\overline{q}}, \overline{\tau}, \dot{\overline{\tau}}\}$ being a small error vector of the state variables at the point of linearization. The coupling can be given by the matrices $J_i \in \mathbb{R}^{2x2}$, $K_i \in \mathbb{R}^{2x2}$, $D_i \in \mathbb{R}^{2x2}$ and $M_{d_i} \in \mathbb{R}^{2x2}$, but out of which only two can be diagonalized simultaneously, e.g., K_i and M_{d_i}.

In order to be able to diagonalize the entire system, we first make the assumption $D_i \approx \lambda_{D_i} K_i$, with λ_{D_i} being a scalar, depending on material properties. As it will become clear in the stability analysis, stability is preserved also for different positive definite matrices D_i. So the error related to this approximation may affect only the transient performance. Furthermore, using the following torque controller

$$\overline{u}_i = J_i(\lambda_{J_i} K_i)^{-1} \overline{w}_i + [\ I - J_i(\lambda_{J_i} K_i)^{-1}\ ]\ (\overline{\tau}_i + D_i K_i^{-1} \dot{\overline{\tau}}_i), \tag{23}$$

one can bring the motor inertia J_i to the form $\lambda_{J_i} K_i$ with λ_{J_i} being a scalar and being chosen so that $\{\parallel J_i(\lambda_{J_i} K_i)^{-1} \parallel -1\} \rightarrow min$. The vector $\overline{w}_i \in \mathbb{R}^2$ is a new control input and $I \in \mathbb{R}^{2x2}$ is the unit matrix. Then, the complete linearized dynamic equations of a coupled joint is given by

$$\overline{w}_i = \lambda_{J_i} K_i \ddot{\overline{\theta}}_i + \overline{\tau}_i + \lambda_{D_i} \dot{\overline{\tau}}_i \tag{24}$$

$$\overline{\tau}_i + \lambda_{D_i} \dot{\overline{\tau}}_i = M_{d_i} \ddot{\overline{q}}_i. \tag{25}$$

Now it is possible to decouple the flexible joint using a modal transformation. Following the lemma 1, there exists a matrix $Q_i \in \mathbb{R}^{2x2}$, such that

$$\begin{cases} K_i &= Q_i Q_i^T \\ M_{d_i} &= Q_i M_{Q_i} Q_i^T \end{cases} \tag{26}$$

holds, with $M_{Q_i} \in \mathbb{R}^{2x2}$ being positive definite and diagonal. By substituting (26) into (24), (25), in modal coordinates one obtains

$$\overline{w}_{Q_i} = \lambda_{J_i} \ddot{\overline{\theta}}_{Q_i} + (\overline{\theta}_{Q_i} - \overline{q}_{Q_i}) + \lambda_{D_i} (\dot{\overline{\theta}}_{Q_i} - \dot{\overline{q}}_{Q_i}) \tag{27}$$

$$(\overline{\theta}_{Q_i} - \overline{q}_{Q_i}) + \lambda_{D_i} (\dot{\overline{\theta}}_{Q_i} - \dot{\overline{q}}_{Q_i}) = M_{Q_i} \ddot{\overline{q}}_{Q_i} \tag{28}$$

with

$$\begin{cases} \overline{\theta}_{Q_i} = Q_i^T \overline{\theta}_i \\ \overline{q}_{Q_i} = Q_i^T \overline{q}_i \\ \overline{w}_{Q_i} = Q_i^{-1} \overline{w}_i. \end{cases} \tag{29}$$

The system (27), (28) is decoupled and for the decoupled subsystems the controller is chosen

$$\overline{w}_{Q_i} = -K_{PQ_i} \overline{\theta}_{Q_i} - K_{DQ_i} \dot{\overline{\theta}}_{Q_i} - K_{TQ_i} (\overline{\theta}_{Q_i} - \overline{q}_{Q_i}) - K_{SQ_i} (\dot{\overline{\theta}}_{Q_i} - \dot{\overline{q}}_{Q_i}).$$

The gain matrices $K_{PQ_i} \in \mathbb{R}^{2x2}$, $K_{DQ_i} \in \mathbb{R}^{2x2}$, $K_{TQ_i} \in \mathbb{R}^{2x2}$, $K_{SQ_i} \in \mathbb{R}^{2x2}$ are positive definite and diagonal. By transforming back into link coordinates, from (26), (29) one obtains

$$\overline{w}_i = -K_{P_i} \overline{\theta}_i - K_{D_i} \dot{\overline{\theta}}_i - K_{T_i} K_i^{-1} \overline{\tau}_i - K_{S_i} K_i^{-1} \dot{\overline{\tau}}_i, \tag{30}$$

with

$$\begin{cases} K_{P_i} = Q_i K_{PQ_i} Q_i^T \\ K_{D_i} = Q_i K_{DQ_i} Q_i^T \\ K_{T_i} = Q_i K_{TQ_i} Q_i^T \\ K_{S_i} = Q_i K_{SQ_i} Q_i^T. \end{cases} \tag{31}$$

All the involved matrices K_{P_i}, K_{D_i}, K_{T_i} and $K_{S_i} \in \mathbb{R}^{2\text{x}2}$ are now positive definite and symmetric.

Furthermore, for a single joint j one can easily determine $\lambda_{J_j} = J_j/K_j$, $\lambda_{D_j} = D_j/K_j$ and $Q_j = \sqrt{K_j}$.

Now, we can generalize the control gain matrices to the entire DLR medical robot, which consists of a single joint {1} and three coupled joint pairs {2-3, 4-5, 6-7}. For the joint stiffness matrix $K \in \mathbb{R}^{7\text{x}7}$ there exist a positive definite and diagonal matrix[1] $\lambda_D \in \mathbb{R}^{7\text{x}7}$ and a block diagonal matrix $Q \in \mathbb{R}^{7\text{x}7}$ as well, so that the conditions

$$K = QQ^T \tag{32}$$

$$D \approx \lambda_D K = \lambda_D QQ^T \tag{33}$$

and

$$\begin{cases} K_P = QK_{PQ}Q^T \\ K_D = QK_{DQ}Q^T \\ K_T = QK_{TQ}Q^T \\ K_S = QK_{SQ}Q^T \end{cases} \tag{34}$$

hold, with all the control gain matrices K_{PQ}, K_{DQ}, K_{TQ} and $K_{SQ} \in \mathbb{R}^{7\text{x}7}$ in modal coordinates being positive definite and diagonal and all the control gain matrices K_P, K_D, K_T, $K_S \in \mathbb{R}^{7\text{x}7}$ in link coordinate being positive definite and symmetric. This property of the control gains is required for the stability analysis in next section.

3.2 *Proposed Control Scheme for the Complete Robot*

From control design using the assumption (33) and the controller (23) to all joints (17), the new robot dynamics is given by

$$w = \lambda_J K\ddot{\theta} + \tau + \lambda_D K\dot{\tau} \tag{35}$$

$$\tau + \lambda_D K\dot{\tau} = M(q)\ddot{q} + C(q,\dot{q})\dot{q} + g(q) \tag{36}$$

$$\tau = K(\theta - q). \tag{37}$$

For this robot dynamics, by completing the linearizing control law (30) we obtain the following controller in link coordinates

$$w = K_P e_\theta - K_D\dot{\theta} + K_T K^{-1} e_\tau - K_S K^{-1}\dot{\tau} + \tau_d \tag{38}$$

with

$$\begin{cases} e_\theta = \theta_d - \theta \\ e_\tau = \tau_d - \tau. \end{cases} \tag{39}$$

Thereby, θ_d and τ_d are the desired motor position and the desired link torque, respectively. In this case the system is considered as an autonomous system and for a given desired link position q_d in the equilibrium point the corresponding desired link torque τ_d and the desired motor position θ_d are given by

$$\tau_d = g(q_d) \tag{40}$$

$$\theta_d = q_d + K^{-1} g(q_d). \tag{41}$$

[1]It is noticed that the diagonal terms of the matrix λ_D with respect to a coupled joint (as well as λ_J) are identical.

3.3 *Stability Analysis*

Theorem 1*: Consider the system (35,36) with the control law (38). For the positive definite and symmetric gains (34), the desired link torque (40), and the desired motor position (41), the controlled system is globally asymptotically stable when the following conditions are satisfied*

$$\begin{cases} \alpha I < Q(I + K_{TQ} + K_{PQ})^{-1} K_{PQ} Q^T \\ K > I\alpha \\ 4\lambda_D I > [(I + K_{TQ})^{-1}(K_{SQ} + \lambda_D I) + \lambda_D I](K_{DQ} + K_{SQ} + \lambda_D I)^{-1}(K_{SQ} + 2\lambda_D I + \lambda_D K_{TQ}). \end{cases}$$

The following lemma [28] will be used for the stability analysis:
Lemma 2 *(positive definite symmetric matrix): Given a symmetric matrix A,*

$$A = \begin{bmatrix} A_{11} & A_{12} \\ A_{12}^T & A_{22} \end{bmatrix}$$

such that every sub-matrix A_{ij} is quadratic, the matrix A is positive definite, if A_{11} is positive definite and $A_{22} \geq A_{12}^T A_{11}^{-1} A_{12}$ holds.

For the proof of stability, we slightly rewrite the equations (35), (36)

$$w = \lambda_J K \ddot{\theta} + K\delta + \lambda_D K \dot{\delta} \tag{42}$$

$$K\delta + \lambda_D K \dot{\delta} = M(q)\ddot{q} + C(q, \dot{q})\dot{q} + g(q) \tag{43}$$

Herein δ is used for $\delta = \theta - q$. The controller (38) is now given by

$$w = K_P e_\theta - K_D \dot{\theta} - K_T \delta - K_S \dot{\delta} + (K + K_T) K^{-1} g(q_d). \tag{44}$$

In order to analyze the system stability the following Lyapunov function candidate is chosen

$$\begin{aligned} V(\theta, \dot{\theta}, q, \dot{q}) = & \frac{1}{2}\dot{\theta}^T K (K + K_T)^{-1} \lambda_J K \dot{\theta} + \frac{1}{2}\dot{q}^T M(q)\dot{q} + \frac{1}{2}(e_\theta - e_q)^T K (e_\theta - e_q) \\ & + \frac{1}{2} {e_\theta}^T K (K + K_T)^{-1} K_P e_\theta + U_g(q) - U_g(q_d) + {e_q}^T g(q_d) \end{aligned} \tag{45}$$

with the link position errors

$$e_q = q_d - q. \tag{46}$$

Equation (45) contains in addition to the motor and link side kinetic energy also the potential energy related to the gravitational vector and to the joint elasticity. Furthermore, the potential energy of the controller is considered.

By using the properties (32), (34) we can obtain that the matrices

$$K(K + K_T)^{-1} \lambda_J K = \lambda_J Q (I + K_{TQ})^{-1} Q^T \quad > 0 \tag{47}$$

$$K(K + K_T)^{-1} K_P = Q(I + K_{TQ})^{-1} K_{PQ} Q^T > 0, \tag{48}$$

are symmetric and positive definite.

Furthermore, from property (P.3) follows

$$\begin{aligned} V \geq\ & \frac{1}{2}\dot{\theta}^T K(K+K_T)^{-1}\lambda_J K\dot{\theta} + \frac{1}{2}\dot{q}^T M(q)\dot{q} + \frac{1}{2}(e_\theta - e_q)^T K(e_\theta - e_q) \\ & + \frac{1}{2}{e_\theta}^T K(K+K_T)^{-1}K_P e_\theta - \frac{1}{2}{e_q}^T \alpha e_q \end{aligned} \tag{49}$$

Since $M(q)$ and $K(K+K_T)^{-1}\lambda_J K$ are positive definite, V is positive, when

$$\begin{aligned} V_A =\ & \frac{1}{2}(e_\theta - e_q)^T K(e_\theta - e_q) + \frac{1}{2}{e_\theta}^T K(K+K_T)^{-1}K_P e_\theta - \frac{1}{2}{e_q}^T \alpha e_q \\ :=\ & \begin{bmatrix} {e_\theta}^T & {e_q}^T \end{bmatrix} H(V_A) \begin{bmatrix} e_\theta \\ e_q \end{bmatrix} \end{aligned} \tag{50}$$

with

$$H(V_A) = \frac{1}{2}\begin{bmatrix} K + K(K+K_T)^{-1}K_P & -K \\ -K & K - \alpha I \end{bmatrix} \tag{51}$$

is positive definite. Accordingly, Hessian $H(V_A)$ has to be positive definite. From Lemma 2 it follows that the conditions

$$\begin{cases} K > \alpha I \\ K - \alpha I > K[K + K(K+K_T)^{-1}K_P]^{-1}K \end{cases}$$

or, equivalently,

$$\begin{cases} K > \alpha I \\ \alpha I < K(K+K_T+K_P)^{-1}K_P < Q(I + K_{TQ} + K_{PQ})^{-1}K_{PQ}Q^T \end{cases} \tag{52}$$

must be fulfilled. Hence the Lyapunov function V is positive.

Then, the derivative of the Lyapunov function V along the system trajectory is

$$\begin{aligned} \dot{V} =\ & \dot{\theta}^T K(K+K_T)^{-1}\lambda_J K\ddot{\theta} + \dot{q}^T M(q)\ddot{q} + \frac{1}{2}\dot{q}^T\dot{M}(q)\dot{q} + (e_\theta - e_q)^T K(-\dot{\theta} + \dot{q}) \\ -\ & {e_\theta}^T K(K+K_T)^{-1}K_P\dot{\theta} + \dot{q}^T g(q) - \dot{q}^T g(q_d). \end{aligned} \tag{53}$$

By substituting (42), (43), (44), (41) in (53) and using the property (P.2), it follows

$$\begin{aligned} \dot{V} =\ & -\dot{\theta}^T K(K+K_T)^{-1}(K_D + K_S + \lambda_D K)\dot{\theta} - \dot{q}^T\lambda_D K\dot{q} \\ & +\dot{\theta}^T[\lambda_D K + K(K+K_T)^{-1}(K_S + \lambda_D K)]\dot{q} \\ \equiv\ & -[\dot{\theta}^T\ \dot{q}^T] \underbrace{\begin{bmatrix} h_{v_{11}} & h_{v_{12}} \\ h_{v_{12}} & h_{v_{22}} \end{bmatrix}}_{H(\dot{V})} \begin{bmatrix} \dot{\theta} \\ \dot{q} \end{bmatrix} \end{aligned} \tag{54}$$

with

$$\begin{cases} h_{11} = K(K+K_T)^{-1}(K_D + K_S + \lambda_D K) = Q(I + K_{TQ})^{-1}(K_{DQ} + K_{SQ} + \lambda_D I)Q^T \\ h_{12} = -\frac{1}{2}[K(K+K_T)^{-1}(K_S + \lambda_D K) + \lambda_D K] = -\frac{1}{2}Q[(I + K_{TQ})^{-1}(K_{SQ} + \lambda_D I) + \lambda_D I]Q^T \\ h_{22} = \lambda_D K = \lambda_D QQ^T. \end{cases}$$

Since all elements of the matrix $H(\dot{V})$ are positive definite and symmetric, according to lemma 2, $\dot{V}$ is negative definite, when the Hessian $H(\dot{V})$ is positive definite or $h_{22} > h_{12}(h_{11})^{-1}h_{12}$. This is equivalent to

$$4\lambda_D I > [(I + K_{TQ})^{-1}(K_{SQ} + \lambda_D I) + \lambda_D I](K_{DQ} + K_{SQ} + \lambda_D I)^{-1}(K_{SQ} + 2\lambda_D I + \lambda_{D_i} K_{TQ}). \quad (55)$$

In case of an autonomous system, the asymptotic stability follows from the invariance principle of Krasovskii-LaSalle. By choosing $\Omega = [\theta, \dot{\theta}, q, \dot{q}]^T$ as a state vector, then the system converges to the largest invariant set contained in the subspace $\Omega = [\theta, 0, q, 0]^T$. From the dynamics (42), (43) and the controller (44) this set is given by

$$K_P e_\theta + (K_T + K)(K^{-1}g(q_d) - \delta) = 0 \quad (56)$$

$$K\delta = g(q). \quad (57)$$

With θ_d from (41) and θ from (57) substituted in (56), one obtains the equilibrium equations

$$g(q) - g(q_d) = K(K_P + K_T + K)^{-1}K_P e_q. \quad (58)$$

From (11) the following relations follow

$$\| g(q_d) - g(q) \| = \| K(K_P + K_T + K)^{-1}K_P e_q \| \leq \alpha \| e_q \| . \quad (59)$$

Regarding (52) it follows that equality is fulfilled only if $q = q_d$. Consequently, $\Omega = \Omega_d = [\theta_d, 0, q_d, 0]$, i.e., the system is globally asymptotically stable.

3.4 *Robustness Analysis*

In this section the robustness of the system is analyzed with respect to inaccuracies from estimates of the joint stiffness matrix, the gravity vector and the friction torque. Firstly, when the estimated friction torque $\hat{\tau}_{fm}$ is used for friction compensation instead of τ_{fm} in (19), then (21) is rewritten

$$\overline{u}_i = J_i\ddot{\overline{\theta}}_i + \overline{\tau}_i + D_i K_i^{-1}\dot{\overline{\tau}}_i + T_i(\tau_{fm_i} - \hat{\tau}_{fm_i}). \quad (60)$$

Now, by using the torque controller (23), the motor dynamics equation (35) can be obtained

$$w = \lambda_J K\ddot{\theta} + \tau + \lambda_D K\dot{\tau} + \rho_{\tau_{fm}} \quad (61)$$

with

$$\rho_{\tau_{fm}} = J^{-1}(\lambda_J K)T(\tau_{fm} - \hat{\tau}_{fm}). \quad (62)$$

Furthermore, the control law (44) requires to know the joint stiffness K and the gravity vector $g(q)$. By considering their uncertainty, the control law can be rewritten as

$$w = K_P e_\theta - K_D\dot{\theta} - K_T\delta - K_S\dot{\delta} + (\widehat{K} + K_T)\widehat{K}^{-1}\widehat{g}(q_d) \quad (63)$$

with $\widehat{K}$ and $\widehat{g}(q)$ being the estimated joint stiffness and gravity vector, respectively. For this control law the desired motor position from (41) is given by

$$\theta_d = q_d + K^{-1}g(q_d) + \rho_q \quad (64)$$

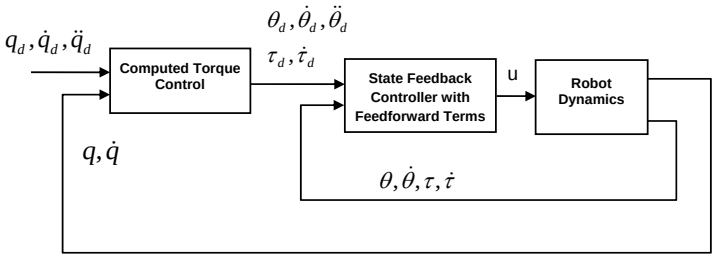

Figure 3. Cascaded control structure.

with

$$\rho_q = \widehat{K}^{-1}\widehat{g}(q_d) - K^{-1}g(q_d). \tag{65}$$

By substituting (63) into (61), one obtains the new equilibrium equation of the motor dynamics

$$K_P e_\theta + (K + K_T)(K^{-1}g(q_d) - \delta) = \rho_g + \rho_{\tau_{fm}} \tag{66}$$

with

$$\rho_g = (K + K_T)K^{-1}g(q_d) - (\widehat{K} + K_T)\widehat{K}^{-1}\widehat{g}(q). \tag{67}$$

Furthermore, substituting (57), (64) into (66) leads to the equilibrium equation

$$g(q_d) - g(q) = -K(K_P + K_T + K)^{-1}K_P(q_d - q) - \rho_\tau \tag{68}$$

with

$$\rho_\tau = K(K_P + K_T + K)^{-1}(K_P\rho_q - \rho_g - \rho_{\tau_{fm}}). \tag{69}$$

From (11), it follows

$$\|g(q_d) - g(q)\| = \| - K(K_P + K_T + K)^{-1}K_P(q_d - q) - \rho_\tau\| \leq I\alpha\|q - q_d\| \tag{70}$$

and therefore its solution lies inside of the interval

$$q \in (q_d - \Gamma^{-1}\rho_\tau, q_d + \Gamma^{-1}\rho_\tau) \tag{71}$$

with

$$\Gamma = K(K_P + K_T + K)^{-1}K_P - I\alpha. \tag{72}$$

4. MIMO state feedback controller with feedforward terms

The MIMO state feedback controller from Sec. 3 is used efficiently with the DLR medical robots. It is very robust and ensures the good dynamic behavior of the robots in the workspace. For medical applications which need high accuracy, a new tracking control scheme is proposed based on the cascaded structure in Fig. 3 with two control loops. Whereas the outer control loop computes the desired references (the desired motor position, the desired link torque and their derivatives) for the inner control loop, the inner control loop uses the MIMO state feedback

controller with feedforward terms to compute the motor torque. Therefor, the desired motor position and the desired link torque are newly computed based on the full rigid body dynamics, and not only on the robot gravity in the equilibrium point. In addition, the desired motor velocity, the derivative of the desired link torque, as well as the desired motor acceleration are used for feedforward terms.

In this section the effect of the joint damping term is neglected and the following reduced dynamics from (35), (36) are now used for control design and stability analysis

$$w = (\lambda_J K)\ddot{\theta} + \tau \tag{73}$$

$$\tau = M(q)\ddot{q} + C(q,\dot{q})\dot{q} + g(q). \tag{74}$$

4.1 *Proposed Tracking Controller*

At first, the inner control loop should be designed to ensure that the link position q converges to the designed link position q_d. In order to enhance the position accuracy, a new MIMO state feedback control law is chosen as

$$w = (\lambda_J K)\ddot{\theta}_d + K_P e_\theta + K_D \dot{e}_\theta + K_T K^{-1} e_\tau + K_S K^{-1} \dot{e}_\tau + \tau_d \tag{75}$$

with the matrix $\lambda_J \in \mathbb{R}^{nxn}$ being positive definite and diagonal (see Sec. 3). All the control matrices K_P, K_D, K_T and $K_S \in \mathbb{R}^{nxn}$ are positive definite and symmetric, and have the same characteristics as the control matrices (34) in Sec. 3.

Then, substituting (75) in (73), we get the closed-loop motor dynamics

$$(\lambda_J K)\ddot{e}_\theta + K_P e_\theta + K_D \dot{e}_\theta + (K_T + K)K^{-1} e_\tau + K_S K^{-1} \dot{e}_\tau = 0. \tag{76}$$

4.2 *Desired References for the Tracking Controller*

The desired link torque τ_d is generated by using the rigid body dynamics [29]. However, an additional control damping term is added to the control law to better damp oscillations of the rigid body dynamics. So for the desired link velocity $\dot{q}_d$ and the desired link acceleration $\ddot{q}_d$, the desired link torque is given by

$$\tau_d = M(q)\ddot{q}_d + C(q,\dot{q})\dot{q}_d + g(q) + K_q \dot{e}_q, \tag{77}$$

where the matrix K_q is positive definite and diagonal.

According to this desired link torque, from (37) the new desired motor position for the controller is given by

$$\theta_d = q_d + K^{-1}[M(q)\ddot{q}_d + C(q,\dot{q})\dot{q}_d + g(q) + K_q \dot{e}_q]. \tag{78}$$

Furthermore, using (77) and (74) we obtain the closed-loop of the link dynamics

$$e_\tau = \tau_d - \tau = M(q)\ddot{e}_q + C(q,\dot{q})\dot{e}_q + K_q \dot{e}_q. \tag{79}$$

4.3 *Stability Analysis*

In contrast to Sec. 3 the system is now considered as a non autonomous system. Therefore, the stability should be analyzed by using Lyapunov's theory and Barbalat's lemma.

Theorem 2: *Consider the system (73,74) with the control law (75). For the positive definite and symmetric gains (34) and the positive definite matrix K_q, the desired link torque (77), and*

the desired motor position (78), the controlled system achieves global asymptotic convergence $\{\lim_{t\to\infty} e_\theta = 0, \lim_{t\to\infty} e_q = 0\}$ *when the following condition is satisfied*

$$K_q > \frac{1}{4}K(K_T + K)^{-1}K_S(K_D + K_S)^{-1}K_S.$$

For stability analysis of the system (73), (74) with the control laws (75), (77), the following Lyapunov function candidate is newly chosen

$$\begin{aligned} V = \ & \frac{1}{2}\dot{e}_\theta^T K(K_T + K)^{-1}(\lambda_J K)\dot{e}_\theta + \frac{1}{2}\dot{e}_q^T M(q)\dot{e}_q + \frac{1}{2}{e_\theta}^T K(K_T + K)^{-1}K_P e_\theta \\ + \ & \frac{1}{2}(e_\theta - e_q)^T K(e_\theta - e_q). \end{aligned} \tag{80}$$

According to (47), (48) the matrices $K(K_T+K)^{-1}(\lambda_J K)$ and $K(K_T+K)^{-1}K_P$ are symmetric and positive definite. Hence the function V is positive definite.

The derivative of the function V along the trajectory, using equations (79) and (76), leads to

$$\begin{aligned} \dot{V} = \ & \dot{e}_\theta^T K(K_T + K)^{-1}(\lambda_J K)\ddot{e}_\theta + \dot{e}_q^T M(q)\ddot{e}_q + \frac{1}{2}\dot{e}_q^T \dot{M}(q)\dot{e}_q + \dot{e}_\theta^T K(K_T + K)^{-1}K_P e_\theta \\ & + (\dot{e}_\theta - \dot{e}_q)^T K(e_\theta - e_q) \\ = \ & - \dot{e}_\theta^T K(K_T + K)^{-1}(K_D + K_S)\dot{e}_\theta + \dot{e}_\theta^T K(K_T + K)^{-1}K_S\dot{e}_q - \dot{e}_q^T K_q \dot{e}_q \\ := \ & -\begin{bmatrix} \dot{e}_\theta^T & \dot{e}_q^T \end{bmatrix} H(\dot{V}) \begin{bmatrix} \dot{e}_\theta \\ \dot{e}_q \end{bmatrix} \end{aligned} \tag{81}$$

with the symmetric Hessian matrix

$$H(\dot{V}) = \begin{bmatrix} K(K_T + K)^{-1}(K_D + K_S) & -\frac{1}{2}K(K_T + K)^{-1}K_S \\ -\frac{1}{2}K(K_T + K)^{-1}K_S & K_q \end{bmatrix}.$$

From (32), (34) it is easy to see that the matrices

$$\begin{aligned} K(K_T + K)^{-1}(K_D + K_S) &= Q(K_{TQ} + I)(K_{DQ} + K_{SQ})^{-1}Q^T > 0 \\ K(K_T + K)^{-1}K_S &= Q(K_{TQ} + I)^{-1}K_{SQ}Q^T > 0 \end{aligned}$$

are positive definite and symmetric.

The function $\dot{V}$ is negative definite when the Hessian matrix $H(\dot{V})$ is positive definite. According to Lemma 2, this leads to the condition

$$K_q > \frac{1}{4}K(K_T + K)^{-1}K_S(K_D + K_S)^{-1}K_S. \tag{82}$$

Therefore, $V > 0$ and $\dot{V} \leq 0$ apply. This implies that $V(t) \leq V(0)$, and that e_θ, $\dot{e}_\theta$, e_q and $\dot{e}_q$ are bounded. Because the derivative of $\dot{V}$ (using equations (79) and (76)) is bounded as well, according to Barbalat's lemma [29] the function $\dot{V}$ is uniformly continuous, or $\dot{V} \to 0$ as $t \to \infty$. That leads to $\{\lim_{t\to\infty} \dot{e}_\theta = 0, \lim_{t\to\infty} \dot{e}_q = 0\}$, hence, $\{\lim_{t\to\infty} \ddot{e}_\theta = 0, \lim_{t\to\infty} \ddot{e}_q = 0\}$. From the closed-loop dynamics (79), (76), it is shown that the position errors converge to zero $\{\lim_{t\to\infty} e_\theta = 0, \lim_{t\to\infty} e_q = 0\}$, or $\{\theta \to \theta_d, q \to q_d\}$.

5. Experiments

In this paper the identification of the coupled joint 2-3 is presented. Furthermore, the performances of the proposed approaches are shown by experiments executed with the coupled joint 2-3 and the whole DLR medical robot. As an example, the tables 1, 2 and 3 represent the parameters of the coupled joint 2-3 obtained from the data sheet, identification and control design.

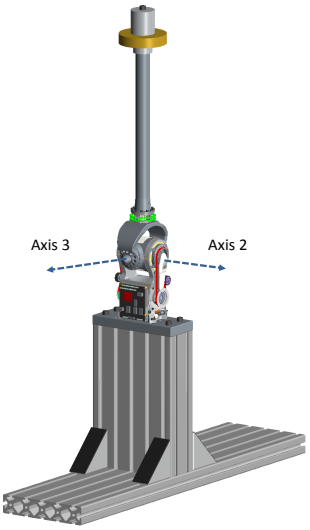

Figure 4. Test-bed setup of the coupled joint 2-3.

Table 1. JOINT PARAMETERS OF THE COUPLED JOINT 2-3.

Motor inertial J_m (kgm^2)	$\begin{bmatrix} 1.26813, & 0.0 \\ 0.0, & 1.26813 \end{bmatrix}$
Stiffness matrix K (Nm/rad)	$\begin{bmatrix} 2700.0, & -101.10 \\ -101.10, & 3035.6 \end{bmatrix}$
Damping matrix D (Nms/rad)	$\begin{bmatrix} 5.06, & -0.59 \\ -0.59, & 7.68 \end{bmatrix}$

Table 2. FRICTION PARAMETERS OF MOTOR 2 and 3.

Motor	f_c (Nm)	f_l	f_v (Nms/rad)	σ_0 (Nm/rad)	σ_1 (Nms/rad)
2	10.51	0.1263	14.56	5033.38	317.66
3	10.36	0.1432	15.48	5423.55	286.50

Table 3. MIMO STATE FEEDBACK CONTROLLER PARAMETERS OF THE COUPLED JOINT 2-3.

K_P	K_D	K_q
$\begin{bmatrix} 7606.33, & 144.33 \\ 144.33, & 7120.02 \end{bmatrix}$	$\begin{bmatrix} 465.08, & 6.61 \\ 6.61, & 442.70 \end{bmatrix}$	$\begin{bmatrix} 0.8, 0.0 \\ 0.0, 0.8 \end{bmatrix}$
$K_T K^{-1}$	$K_S K^{-1}$	$\{\lambda_J, \ \lambda_D\}$
$\begin{bmatrix} 6.04824, 0.08149 \\ 0.08143, 5.77639 \end{bmatrix}$	$\begin{bmatrix} 0.004742, & -0.006841 \\ -0.006837, & 0.027564 \end{bmatrix}$	$\begin{bmatrix} 0.001, 0.00064 \end{bmatrix}$

5.1 *Identification of the Elasticity*

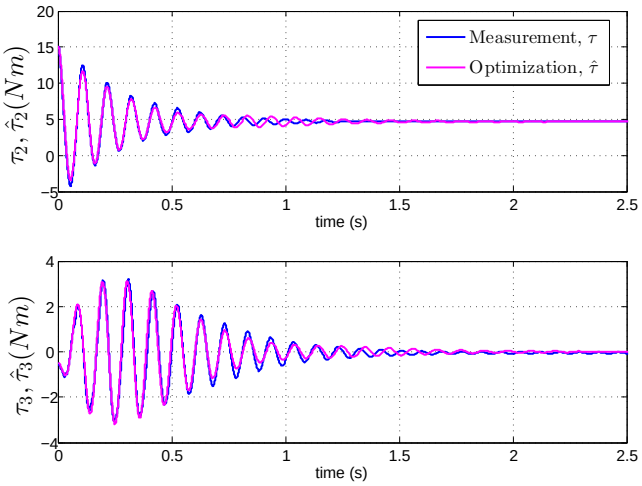

Figure 5. Measured and modeled link torques with optimized values of the elasticity in link coordinates when joint 2 is excited to oscillate.

The coupled joint 2-3 should be excited to oscillate as a two link system and the joint torque oscillations are recorded in the time domain. Therefore, it is position controlled with high desired velocity in the direction of joint 2. Then, in dedicated positions the controller is turned off and the motor brake is activated. Because of the joint elasticity the link masses start to oscillate. Due to the joint coupling the mechanical oscillations occur not only in the main axis 2, but also in its cross axis 3 (in Fig. 5).

For fixed motor shaft, $\theta = \theta_0 \in \mathbb{R}^2$ is constant and the link dynamic equation generally reduces to

$$\hat{\tau} - D\dot{q} = \overline{M}(q)\ddot{q} + \overline{C}(q,\dot{q})\dot{q} + \overline{g}(q) \tag{83}$$

$$\hat{\tau} = K(\theta_0 - q). \tag{84}$$

Hereby, $\overline{M} \in \mathbb{R}^{2x2}, \overline{v} \in \mathbb{R}^2, \overline{g} \in \mathbb{R}^2$ are determined by using the rigid body parameters from the CAD model and given by

$$\overline{M}(q) = \begin{bmatrix} a_1 \sin(q_3)^2 + a_2 \cos(q_3)^2 \ , & 0.0 \\ 0.0 & , \quad a_3 \end{bmatrix}; \quad \overline{C}(q,\dot{q}) = \begin{bmatrix} b_1 \sin(q_3)\cos(q_3)\dot{q}_3 \ , & b_2 \sin(q_3)\cos(q_3)\dot{q}_2 \\ b_3 \sin(q_3)\cos(q_3)\dot{q}_2 \ , & 0 \end{bmatrix}$$

$$\overline{g}(q) = \begin{bmatrix} c_1 \sin(q_2)\cos(q_3) \\ c_2 \sin(q_3)\cos(q_2) \end{bmatrix}.$$

The joint stiffness matrix $K \in \mathbb{R}^{2x2}$ and the joint damping matrix $D \in \mathbb{R}^{2x2}$ are determined by minimizing the torque error between measurement $\tau \in \mathbb{R}^2$ and simulation $\hat{\tau} \in \mathbb{R}^2$ in (83) (using nonlinear least-squares method)[1]

$$\|\tau - \hat{\tau}\|_2 \to 0. \tag{85}$$

The identification results for the elasticity of the joint 2-3 are shown in Fig. 5 and table 1.

[1]This equation is minimized by using the "lsqnonlin" function (solve nonlinear least-squares) from the matlab optimization toolbox.

5.2 *Identification of the Friction*

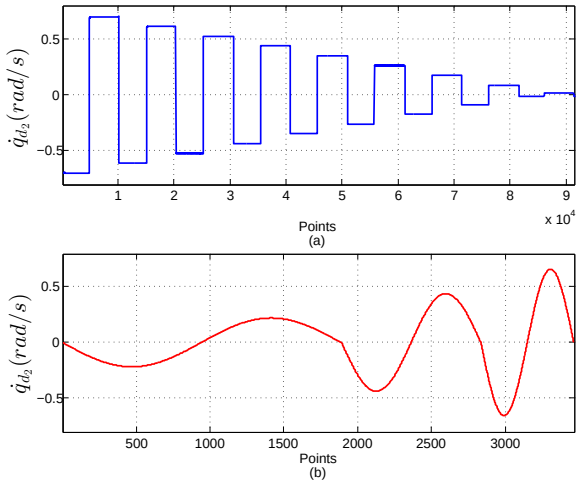

Figure 6. Desired velocity profile of the joint 2 in link coordinates for the identification of the static friction parameters (a) and the dynamic friction parameters (b).

The LuGre friction parameters can be classified into two groups:

- the static friction parameters f_c, f_v, f_l and
- the dynamic friction parameters σ_0, σ_1.

They are identified by minimizing the error between the model based computed motor current $\widehat{I}_m$ and the commanded current from the controller I_m (using nonlinear least-squares method)[1], so that

$$\|I_m - \widehat{I}_m\|_2 \to 0. \tag{86}$$

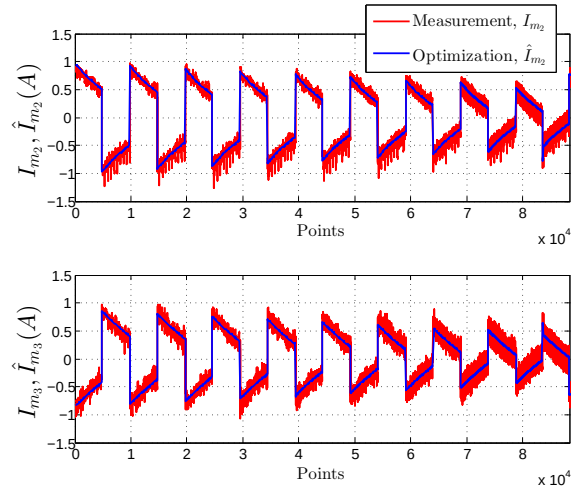

Figure 7. Comparison of measured and simulated motor currents by the static friction identification in motor coordinates.

At first, the static friction parameters f_c, f_v and f_l are determined by the steady-state friction force when the velocity is held constant. For steady-state motion, when $\dot{\theta}_m = const$ (e.g. different

[1]This equation is minimized by using the "fmincon" function (find minimum of constrained nonlinear multivariable function) from the matlab optimization toolbox in case of the static friction parameters and the "lsqnonlin" function in case of the dynamic friction parameters.

velocities from 1 to 40 deg/s in Fig. 6.a), it follows from (14) that z is exponentially convergent and $\lim_{t\to 0} \dot{z} = 0$. Hence, the friction force is given by

$$\tau_{fm} = (f_c + f_l|\tau_m|)sign(\dot{\theta}_m) + f_v\dot{\theta}_m \mid_{\dot{z}=0} \tag{87}$$

and from (5), (6) the motor current is

$$\widehat{I}_m \simeq K_{T2I}(T^T(\tau + DK^{-1}\dot{\tau}) + \tau_{fm}) \mid_{\dot{z}=0,\ \dot{\theta}_m=const} . \tag{88}$$

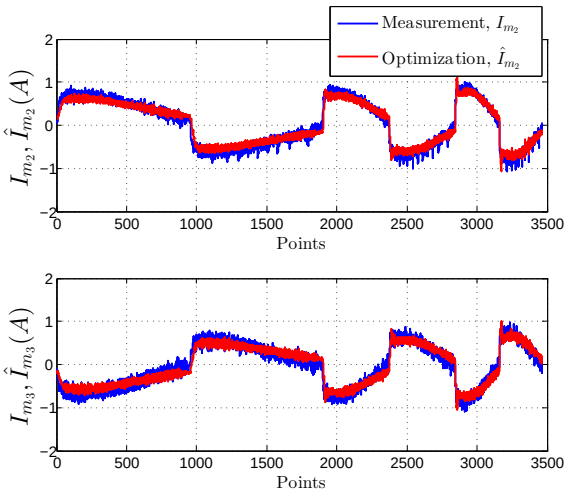

Figure 8. Comparison of measured and simulated motor currents by the dynamic friction identification in motor coordinates.

Next, the dynamic friction parameters $\sigma_0,\ \sigma_1$ are identified by using a desired sine trajectory with different frequencies (e.g. [0.08, 0.14, 0.24] Hz in Fig. 6.b). Thus, the friction force is given by

$$\tau_{fm} = \sigma_0 z + \sigma_1 \dot{z} + f_v\dot{\theta}_m \tag{89}$$

and the motor current is

$$\widehat{I}_m \simeq K_{T2I}(J_m\ddot{\theta}_m + T^T(\tau + DK^{-1}\dot{\tau}) + \tau_{fm}). \tag{90}$$

Then, all friction parameters are identified by minimizing the motor current error (86) using (88) for the static friction parameters and (90) for the dynamic friction parameters. In order to improve the identification results, the regions with overshooting signals at reversal points of the trajectory are excluded from the measured data used for optimization.

The identification results of the LuGre friction model of the joint coupled 2-3 are shown in Fig. 7, Fig. 8 and table 2.

5.3 *Control Validation*

At first, the control performance in terms of the dynamic behavior of the proposed MIMO state feedback controller from Sec. 3 is validated by comparing *step response* results with the PD controller [3] and the SISO state feedback controller [6] (by neglecting the joint coupling). The experiment "step response" with a step of 5 deg is independently executed with respect to joint 2 and joint 3. Fig. 9 and Fig. 10 present the experimental results respectively. Obviously, the MIMO state feedback controller exhibits strongly damped oscillations of the measured link torques in both, the excited and the coupled axis. Especially, for the PD controller only limited

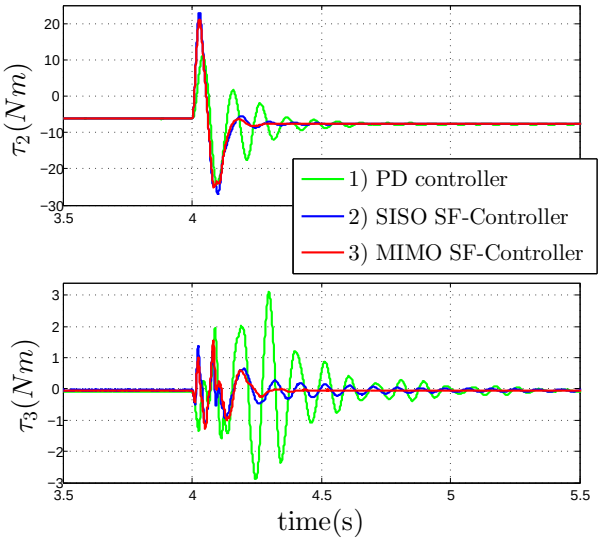

Figure 9. Measured link torque in link coordinates after a step of joint 2 with: 1) PD controller; 2) SISO state feedback controller; 3) MIMO state feedback controller.

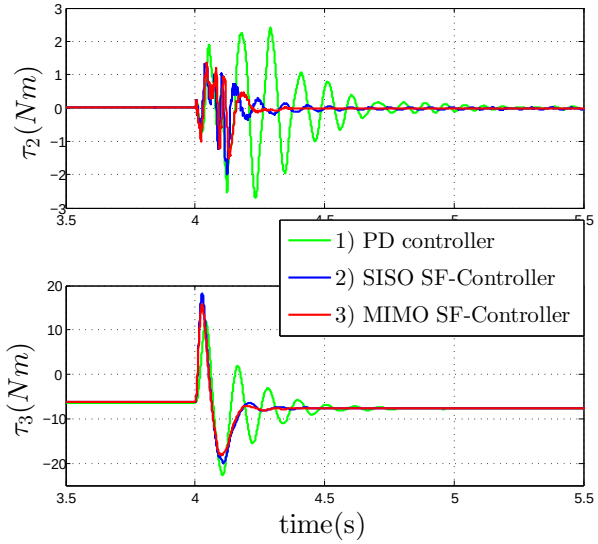

Figure 10. Measured link torque in link coordinates after a step of joint 3 with: 1) PD controller; 2) SISO state feedback controller; 3) MIMO state feedback controller.

performance can be achieved because the feedback is restricted to motor state variables only, without using link side information such as link position or link torque.

Next, the control performance of the MIMO state feedback controller with feedforward terms from Sec. 4 is compared with the PID controller and the MIMO state feedback controller without feedforward terms from Sec. 3. The experiments are performed with the coupled joint 2-3 with different desired trajectories.

In a first experiment, the coupled joint 2-3 follows a periodic trajectory (see Fig. 11) in order to show the performance in terms of the position accuracy and the dynamic behavior. Fig. 12 shows that the MIMO state feedback controller with feedforward terms achieves a lower position accuracy than the PID controller. However, concerning the dynamic behavior at the reversal points of the trajectory, the PID controller causes strong oscillations of the measured link torques (Fig. 13), whereas the MIMO state feedback controller with feedforward terms causes a higher peak due to the desired link acceleration (which can be reduced if the desired link acceleration at the reversal points of the trajectory is smoothed), but almost no oscillation. In this case the MIMO state feedback controller without feedforward terms shows the best results with strongly

damped oscillations of the measured link torques.

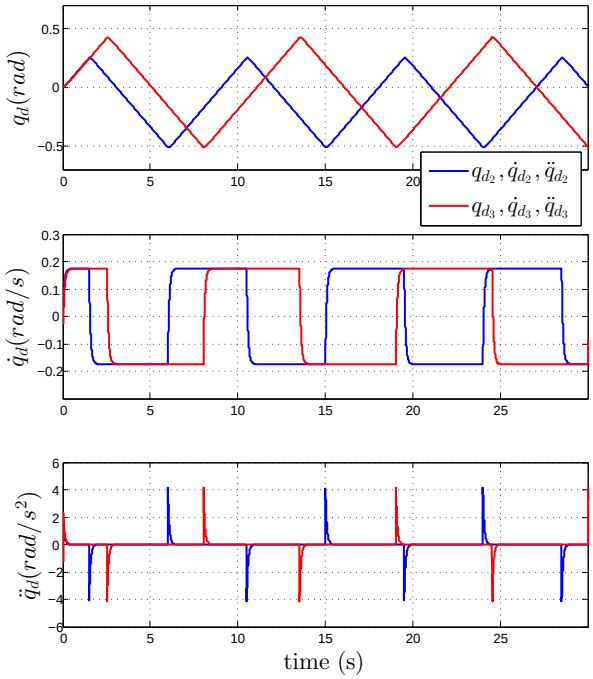

Figure 11. Desired link position, velocity, and acceleration of a periodic trajectory for joints 2 and 3 in link coordinates.

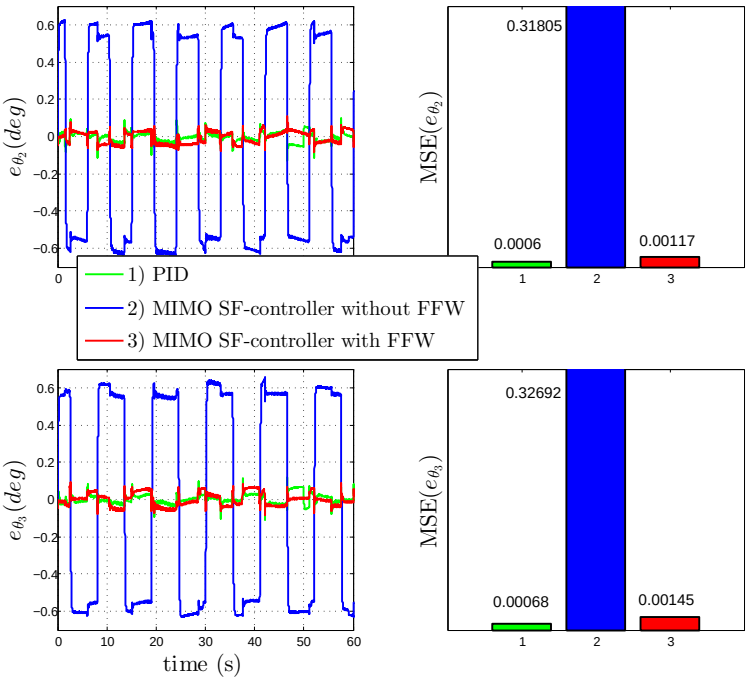

Figure 12. Tracking motor position errors in link coordinates and their MSE (squared error performance) during the periodic trajectory with: 1) PID controller; 2) MIMO state feedback controller without feedforward; 3) MIMO state feedback controller with feedforward.

In a second experiment, the coupled joint 2-3 follows a point to point trajectory (Fig. 14) in order to show the position accuracy. Obviously, the MIMO state feedback controller with feedforward terms shows a quite good result as well (Fig. 15).

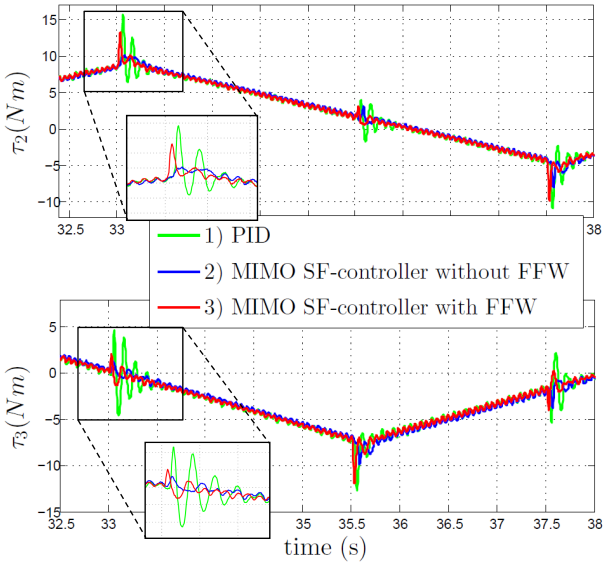

Figure 13. Measured link torque in link coordinates during the periodic trajectory with: 1) PID controller; 2) MIMO state feedback controller without feedforward; 3) MIMO state feedback controller with feedforward.

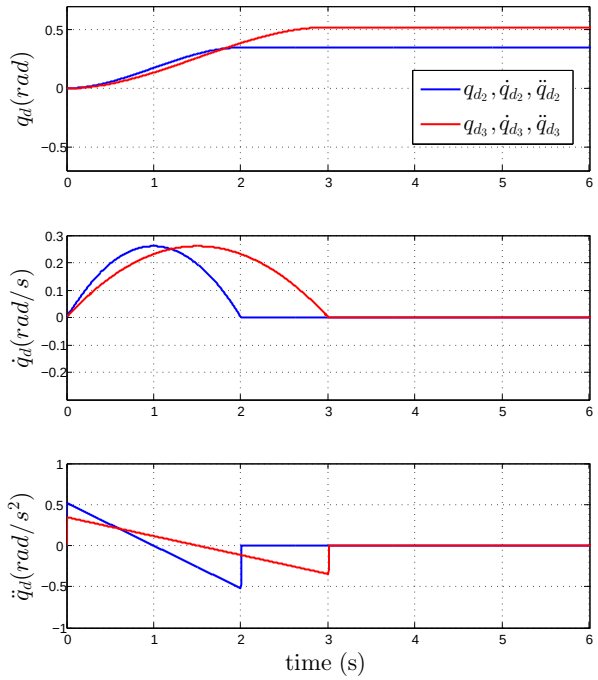

Figure 14. Desired link position, velocity, acceleration of a point to point trajectory for joints 2 and 3 in link coordinates.

Furthermore, the robustness of the MIMO state feedback controller without feedforward terms is validated against uncertainties of the desired link torques τ_d (dependent on the load) and the desired friction torque for friction compensation. By using the same desired trajectory as in Fig. 11, Fig. 16 and Fig. 17 show the motor position errors when the desired link torque τ_d is changed from 50% to 100% of its identified value and when the desired friction torque $\hat{\tau}_{fm}$ is changed from 0% to 100% of its identified value, respectively. It can be seen that the controlled system is very robust and keeps stability against these disturbances.

Finally, some experiments were executed with the complete DLR medical robot. Let us introduce the forward kinematics of the robot as $x = f(q) \in \mathbb{R}^6$, then the Cartesian position errors are defined $e_{cart} = f(q_d) - f(q) \in \mathbb{R}^6$. Since the PID controller causes the strong structural

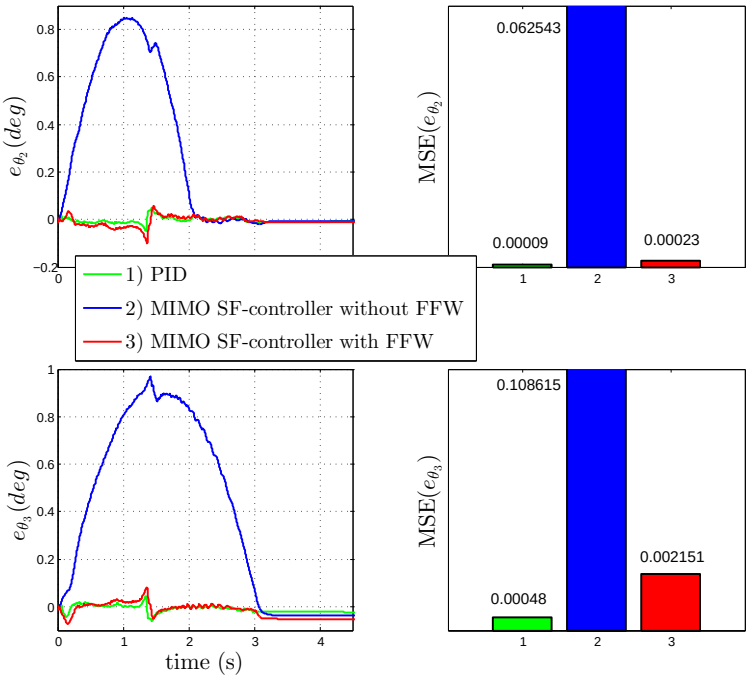

Figure 15. Tracking motor position errors in link coordinates and their MSE (squared error performance) during the point to point trajectory with: 1) PID controller; 2) MIMO state feedback controller without feedforward; 3) MIMO state feedback controller with feedforward.

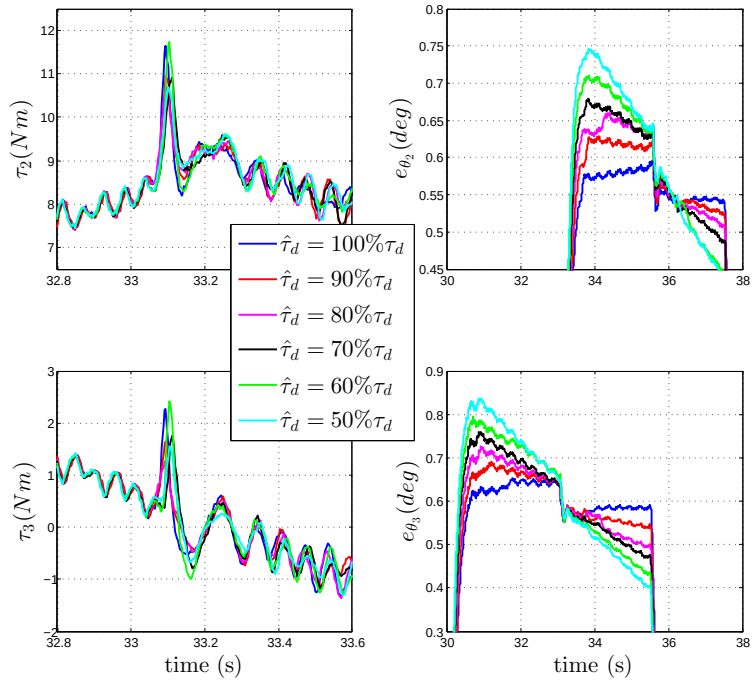

Figure 16. Link torques and tracking motor position errors of the MIMO state feedback controller without feedforward in link coordinates when the desired link torque varies.

oscillations due to its high joint elasticity, high ripple-effects (of the Harmonic drive and the BLDC motor), and high motor friction, it cannot be used in practice for the DLR medical robot. Therefore, only the Cartesian position errors (Fig. 19) of the MIMO state feedback controller with- and without feedfordward are compared, when the robot tracks the Cartesian designed trajectory of Fig. 18. It can be seen that the MIMO state feedback controller with feedforward terms improves the tracking position accuracy.

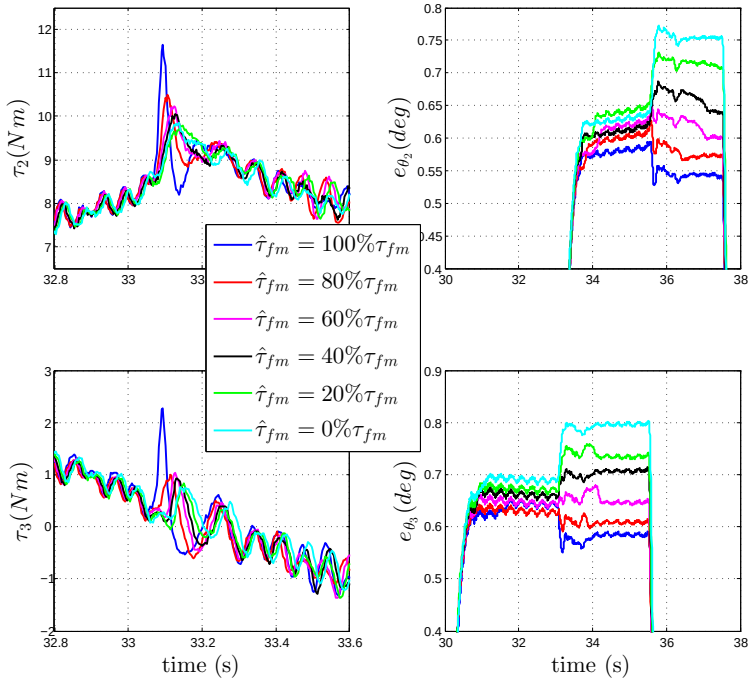

Figure 17. Link torques and tracking motor position errors of the MIMO state feedback controller without feedforward in link coordinates when the desired friction torque varies.

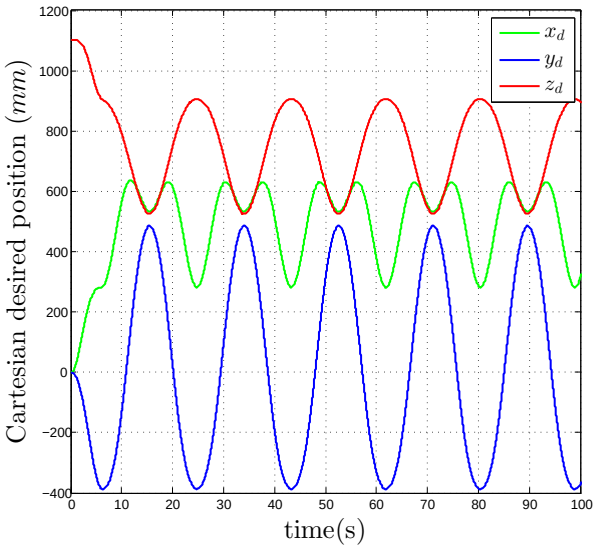

Figure 18. Desired Cartesian position for the DLR Miro robot.

Although the proposed tracking controller considerably contributes to the reduction of the positioning errors and the joint oscillations, in the experiments small steady state errors can be seen because the effects of the unmodeled dynamics (the friction model and the rigid body dynamics) are not completely compensated. Theoretically this can be solved by adaptive control, but this goes beyond the scope of this work.

6. Conclusion

In this paper, a MIMO state feedback controller for the DLR medical robot has been designed through modal decomposition in order to deal with the high coupling between the robot joints.

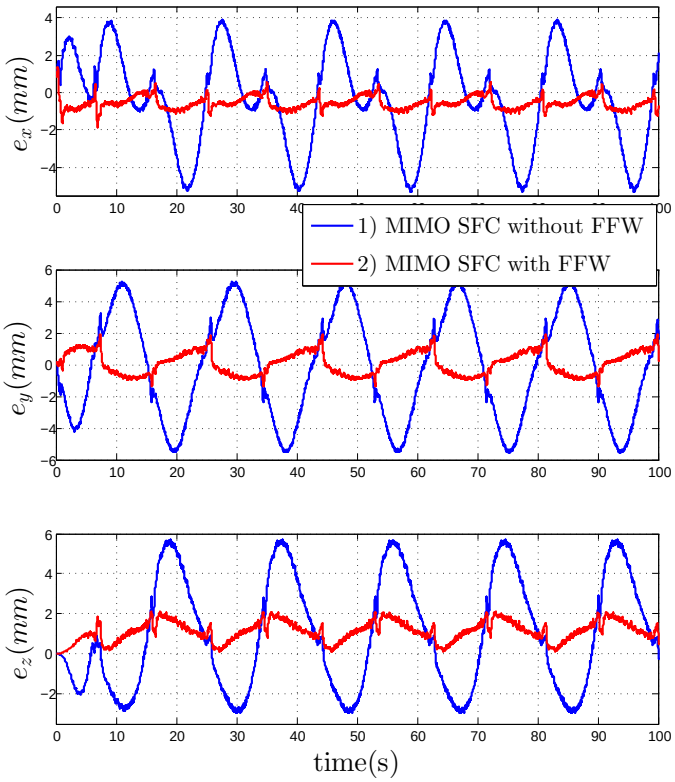

Figure 19. Tracking Cartesian position errors for the DLR medical robot: 1) MIMO state feedback controller without feedforward; 2) MIMO state feedback controller with feedforward.

Furthermore, a tracking cascaded control scheme has been developed based on the MIMO state feedback controller with additional feedforward terms, which achieves good performance in terms of the position accuracy and the dynamic behavior. Stability analysis is shown based on Lyapunov's theory. Finally, experimental results validate the proposed approaches for the DLR medical robot.

References

[1] U. Hagn, M. Nickl, S. Jörg, G. Passig, T. Bahls, A. Nothhelfer, F. Hacker, L. Le-Tien, A. Albu-Schäffer, R. Konietschke, M. Grebenstein, R. Warpup, R. Haslinger, M. Frommberger, G. Hirzinger. The DLR MIRO: A versatile lightweight robot for surgical applications. Industrial Robot: An International Journal. 2008. p. 324–336.

[2] T. Ortmaier, H. Weiss, U. Hagn, M. Grebenstein, M. Nickl, A. Albu-Schäffer, C. Ott, S. Jörg, R. Konietschke, L. Le-Tien, G. Hirzinger. A Hands-On-Robot for Accurate Placement of Pedicle Screws. ICRA. 2006. p. 4179–4186.

[3] P. Tomei. A simple PD Controller for Robots with Elastic Joints. IEEE Transaction on Robotics and Automation; 1991. p. 1208–1213.

[4] A. De Luca, B. Siciliano, L. Zollo. PD control with on-line gravity compensation for robots with elastic joints: Theory and experiments. Automatica. 2005;41:1809-1819.

[5] M. J. Kim, W. K. Chung. Disturbance-Observer-Based PD Control of Flexible Joint Robots for Asymptotic Convergence. IEEE Transactions on robotics. 2015;31:6: p. 1508–1516.

[6] A. Albu-Schäffer, G. Hirzinger. A Globally Stable State-feedback Controller for Flexible Joint Robots. Journal of Advanced Robotics. 2001. p. 799–814.

[7] G. Hirzinger, N. Sporer, A. Albu-Schäffer, M. Hähnle, R. Krenn, A. Pascucci, M. Schedl. DLR's torque-controlled light weight robot III - are we reaching the technological limits now?. ICRA. 2002. p. 1710–1716.

[8] B. Siciliano, L. Villani. Two-Time Scale Force and Position Control of Flexible Manipulators. ICRA.

2001. p. 2729–2734.
[9] H. D. Taghirad, M. A. Khorsavi. A Robust Linear Controller for Flexible Joint Manipulators. IEEE/RSJ International Conference on Intelligent Robots and Systems. 2004. p. 2936-2941.
[10] B. Brogliato, R. Ortega, R. Lozano. Global Tracking Controllers for Flexible-Joint Manipulators: a Comparative Study. Automatica. 1995;31:941–956.
[11] J. Lee, J S. Yeon, J. H. Park, S. Lee. Robust Back-Stepping Control for Flexible-Joint Robot Manipulators.IEEE/RSJ International Conference on Intelligent Robots and Systems. 2007; p. 183–188.
[12] A. De Luca, P. Lucibello. A General Algorithm for Dynamic Feedback Linearization of Robots with Elastic Joints. ICRA. 1998. p. 504–510.
[13] L. Tian, A.A. Goldenberg. Robust Adaptive Control of Flexible Joint Robots with Joint Torque Feedback. ICRA. 1995. p. 1229-1234.
[14] A. Kugi, C. Ott, A. Albu-Schaffer, G. Hirzinger. On the passivitybased impedance control of flexible joint robots. IEEE Transactions on Robotics. 2008;24:2: p. 416-429.
[15] C.-I. Morarescu, B. Brogliato. Passivity-based switching control of flexible-joint complementarity mechanical systems. Automatica. 2010;46:1: p. 160-166.
[16] K. Melhem, W. Wang. Global output tracking control of flexible joint robots via factorization of the manipulator mass matrix. IEEE Transaction on robotics. 2009;25:2: p. 428–437.
[17] A. Mohammadi, M. Tavakoli, H. J. Marquez, and F. Hashemzadeh. Nonlinear disturbance observer design for robotic manipulators. Control Engineering Practice. 2013; 21:3: p. 253–267.
[18] J. Huang, S. Ri, L. Liu, Y. Wang, J. Kim, G. Pak. Nonlinear Disturbance Observer-Based Dynamic Surface Control of Mobile Wheeled Inverted Pendulum. IEEE Trans on Control Systems Technology. 2015; 23:6: p. 2400–2407.
[19] W.-H. Chen. Disturbance observer based control for nonlinear systems. IEEE/ASME Transaction on Mechatronics. 2004; 9:4: p. 706–710.
[20] S. Ibrir. Nonlinear observer design with robustness of transient behavior: Application to a flexible-joint robot. IEEE International Conference on Control Applications Part of 2010 IEEE Multi-Conference on Systems and Control. 2010; p. 1385–1390.
[21] J. Lee, T. J. Hal, J. S. Yeon, S. Lee, J. H. Park. Robust Nonlinear Observer for Flexible Joint Robot Manipulators with Only Motor Position Measurement. International Conference on Control, Automation and Systems. 2007; p. 17–20.
[22] W. E. Dixon, E. Zergeroglu, D. M. Dawson, M. W. Hannan. Global adaptive partial state tracking control of rigid-link flexible-joint robots. Robotica. 2000:18: p. 325-336.
[23] C. Kwan, K. S. Yeung. Robust adaptive control of revolute flexible-joint manipulators using sliding technique. Systems & Control Letters. 1993;20: p. 279–288.
[24] C. C. de Wit and H. Olsson, K. J. Astron, P. Linschinsky. A New Model for Control of Systems with Friction. IEEE Transaction on Automatic Control. 1994;40: p. 419–425.
[25] L. Le-Tien, A. Albu-Schäffer. Adaptive Friction Compensation in Trajectory Tracking Control of DLR Medical Robots with Elastic Joints. IROS. 2012.
[26] L. Le-Tien, A. Albu-Schäffer, G. Hirzinger. MIMO State Feedback Controller for a Flexible Joint Robot with Strong Joint Coupling. ICRA. 2007. p. 3824–3830.
[27] L. Le-Tien, A. Albu-Schäffer. Improving Tracking Accuracy of a MIMO State Feedback Controller for Elastic Joint Robots. 53rd IEEE Conference on Decision and Control. 2014. p. 4548–4553.
[28] Stephen Boyd, Lieven Vandenberghe. Convex Optimization. 2004.
[29] J-J. E. Slotine, W. Li. Applied Nonlinear Control. 1991.
[30] R. A. Horn, C. R. Johnson. Matrix Analysis. Cambridge University Press. 1985.

Appendix A. Computation of the Constant α

In order to determine the equation (52), we need to determine α. The upper limit of the constant α can be computed based on the fact that

$$\frac{\partial g_i(q)}{\partial q_j} \leq g_{i_{max}} \tag{A1}$$

with $g_{i_{max}}$ being the maximal moment which can be exerted in axis i by the gravitational force. Since the gravity vector is a continuous function of the joint position, from the "*mean value theorem*" there exists a q_δ with $q_2 < q_\delta < q_1 \in \mathbb{R}^n$ so that

$$[g_i(q_1) - g_i(q_2)]^2 = |\frac{\partial g_i(q)}{\partial q}|_{q=q_\delta}(q_1 - q_2)|^2 = \| \frac{\partial g_i(q)}{\partial q}|_{q=q_\delta}(q_1 - q_2) \|^2$$
$$\leq \| \frac{\partial g_i(q)}{\partial q}|_{q=q_\delta} \|^2 \| q_1 - q_2 \|^2 \leq n g_{i_{max}}^2 \| q_1 - q_2 \|^2 \qquad \forall i = 1..n. \quad \text{(A2)}$$

Therefore, it follows

$$\| g_i(q_1) - g_i(q_2) \| = \sqrt{\sum_{i=1}^{n} [g_i(q_1) - g_i(q_2)]^2} \leq \sqrt{n \sum_{i=1}^{n} g_{i_{max}}^2} \| q_1 - q_2 \| \quad \text{(A3)}$$

or

$$\alpha = \sqrt{n \sum_{i=1}^{n} g_{i_{max}}^2}. \quad \text{(A4)}$$